1310-nm Hybrid III–V/Si Fabry–Pérot Laser Based on Adhesive Bonding

Stevan Stanković, *Member, IEEE*, Richard Jones, *Member, IEEE*, Matthew N. Sysak, *Member, IEEE*,
John M. Heck, *Member, IEEE*, Günther Roelkens, *Member, IEEE*, and Dries Van Thourhout, *Member, IEEE*

Abstract—An evanescently coupled, hybrid III–V/Silicon Fabry–Pérot laser based on adhesive divinyl siloxane-benzocyclobutene (DVS-BCB) bonding is presented operating at 1310 nm. We obtain 5.2-mW output power in continuous-wave (CW) regime at 10 °C with a threshold current density of 2.83 kA/cm^2 in an 800-μm-long device. A specially developed bonding procedure produces 50-nm-thick bonding layers, enabling the evanescent coupling.

Index Terms—Evanescent coupling, heterogeneous integration, semiconductor lasers, silicon photonics.

I. INTRODUCTION

SILICON photonics is a rapidly-developing technology on the silicon-on-insulator (SOI) material platform using the fabrication processes and tools of microelectronics. This technology promises to enable the cost-effective fabrication of high-performance photonic integrated circuits and the co-integration of electronic devices on a single chip. However, due to silicon's indirect bandgap, fabrication of efficient light sources in silicon photonics still remains a serious challenge.

The heterogeneous integration of III–V materials and SOI waveguides is an appealing approach to this problem promising a high density integration and avoiding the need for costly active alignment that is needed in the case of packaged lasers. State-of-the-art hybrid lasers in this field are mostly based on evanescent coupling which offers a simple and effective way to couple the laser emission into the SOI waveguide and requires no complex coupling structures (such as narrow-tip tapers [1]), which are challenging for fabrication. On the other hand, due to the lower optical confinement factor in the active region, these devices have longer lengths and higher threshold currents. Previously demonstrated, evanescently coupled hybrid lasers include Fabry–Pérot [2]–[4], distributed Bragg reflector (DBR) [5], and distributed feedback (DFB) lasers [6]. These devices were based on a molecular (direct) wafer bonding technique which requires very clean, smooth and contamination-free
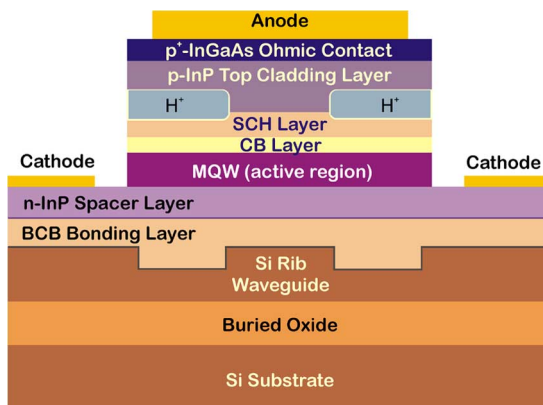
Fig. 1. Cross-section of an evanescent, hybrid III–V/Si laser based on DVS-BCB bonding.

surfaces. Such strict requirements could raise challenges to an industrial-scale fabrication of these lasers. Alternatively, an evanescent hybrid III–V/Si laser based on selective-area metallic bonding was reported [7]. Although it offers more relaxed bonding requirements, this technique requires very precise alignment of the prefabricated III–V and SOI dies, which is a serious drawback from the aspect of high-level integration.

In this letter, we study an alternative approach based on adhesive bonding, using the commercially available DVS-BCB polymer. The DVS-BCB bonding have been recently used for fabrication of photodetectors and hybrid III–V/Si lasers with adiabatic inverted tapers [8], but before this work, this bonding process was not considered suitable for the realization of evanescent hybrid lasers due to the thick ($>$100 nm) adhesive layers which dramatically decrease the optical confinement in the gain material. In this letter we show that adhesive bonding is a viable approach and we present the design and fabrication procedure of a hybrid Fabry–Pérot III–V/Silicon evanescent laser operating at 1310 nm, based on DVS-BCB adhesive bonding.

II. HYBRID LASER DESIGN

The cross-section of the hybrid III–V/Silicon evanescent laser is shown in Fig. 1. The silicon rib waveguide is made on the SOI platform, with a 1 μm thick buried oxide layer. The waveguide height and width are 500 nm and 0.8 μm, respectively. The rib etch depth is 220 nm and the width of the surrounding trenches is 3.5 μm. The epitaxial III–V structure is bonded on top of the waveguide, using DVS-BCB as an adhesive. It comprises the n-type InP spacer layer and the 16.8 μm wide mesa structure made of the multiple quantum
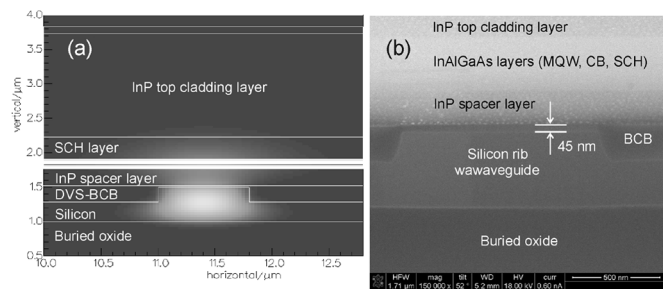
Fig. 2. (a) Simulated profile of the fundamental optical hybrid mode supported by the laser cavity; (b) SEM of the cross-section of a III–V die bonded on a Si rib waveguide with a 45-nm-thick DVS-BCB bonding layer.

Fig. 3. L–I plots of the 600 and 800 μm-long hybrid lasers in CW regime.

well (MQW) region (8 InGaAlAs-based QWs and 9 barriers), carrier blocking (CB) layer, a separate confinement heterostructure (SCH) layer, a p-type InP top cladding layer and an ohmic contact. Both CB and SCH layers are based on InAlGaAs alloys, while the ohmic contact is made from heavily p-type doped InGaAs. For efficient evanescent coupling between the modes supported by the III–V layers and the silicon rib waveguide, the thickness of the DVS-BCB bonding layer must be sufficiently small, i.e. less than 100 nm. The device is designed to support the fundamental hybrid optical TE mode which is predominantly confined within the Si waveguide, with only a fraction of the optical power within the MQW active region (as shown in Fig. 2(a)).

Using a full-vectorial mode solver, the optimal thicknesses of the n-type spacer layer and the SCH layer were found to be 240 nm and 325 nm, respectively. For these values the laser design is tolerant to variations in BCB layer thickness, yielding confinement factors for the fundamental mode within the Si waveguide (Γ_{Si}) and within the MQW active regions (Γ_{MQW}) of more than 70% and 3%, respectively, in a range of BCB bonding layer thicknesses between 20 nm and 120 nm. In order not to excite higher order modes, which are more broadly distributed in the mesa, the current injection is confined using proton implantation in the lateral sections of the mesa (as shown in Fig. 1).

III. DEVICE FABRICATION

Fabrication starts with the bonding of an unprocessed III–V die onto a SOI die containing the rib waveguides. In our approach, DVS-BCB is spin-coated on the patterned SOI die, after which the III–V die is brought into contact with it and the DVS-BCB is cured. For this purpose, we developed a die-to-die bonding process for achieving thin ($\sim$50 nm) DVS-BCB bonding layers [9]. This is illustrated in Fig. 2(b), which shows an SEM image of a cross-section of the III–V die bonded on top of the SOI waveguide, using this procedure. After the bonding, the InP substrate is removed by combination of grinding and wet-etching.

Processing of the bonded III–V die starts with the definition of III–V islands, galvanically separating individual lasers, by using contact lithography and wet etching techniques. Mesa structures are fabricated combining dry etching and wet etching processes, after which the n-type metallization (Au–Ge–Ni alloy system) is deposited. In the next step, DVS-BCB is
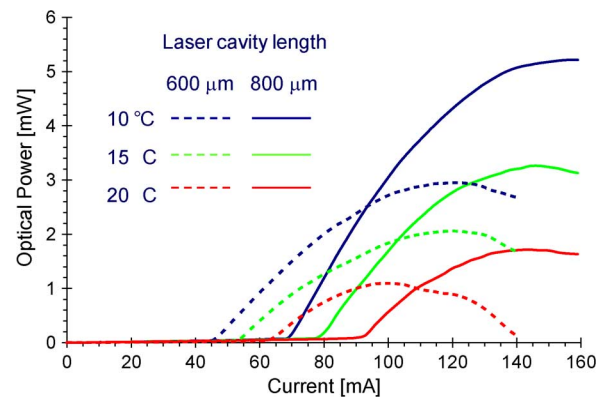
spin-coated on the sample and cured, providing a physical protection and electrical isolation between the electrodes. Dry etching is used to make vias in the DVS-BCB covering layer for n-type and p-type contacts. P-type metallization is performed by sputtering a thin Ti layer, followed by the deposition of a 1.2 μm-thick Au layer. The thick P-type electrodes also serve as the mask for subsequent proton implantation which is used to increase electrical resistivity in the lateral regions of the mesa and confine the injected current to the central region of the mesa where the secondary peak of the fundamental hybrid mode is located. The width of the central P-type electrode, which allows the formation of the carrier injection channel, is 3 μm, while the length of the devices varied from 500 μm to 900 μm. In the last step, gold is deposited on the electric contacts, after which the individual devices are cleaved (or diced and polished) and tested.

IV. RESULTS

The cleaved devices are tested with DC and pulse current sources. The output power of the laser is measured at one facet of the device using a large-area photodetector positioned in close proximity to the facet, so that practically all the emitted optical power from one facet is detected. Devices are mounted on a copper plate and its temperature stabilization is achieved using a Peltier element. Typical L–I plots in CW regime, for 600 μm and 800 μm-long lasers, at temperatures of 10 °C, 15 °C, and 20 °C are given in Fig. 3. For a 800 μm-long device, the threshold current at 20 °C is 92 mA (corresponding to a current density of 3.83 kA/cm^2), the maximum optical power at 20 °C is 1.71 mW, while the slope efficiency is $\sim$0.05 W/A. At 10 °C, the threshold current is 68 mA (2.83 kA/cm^2), the maximum optical output power is 5.21 mW and the slope efficiency rises to 0.1 W/A. The 600-μm long laser, has a threshold current of 64 mA (3.55 kA.cm^2) at 20 °C and the maximum optical power 1.09 mW, while at 10 °C the threshold current is 45 mA (2.50 kA/cm^2) and the maximum optical power is 2.95 mW. Typical L–I plots for devices in pulse regime (5% duty cycle, 100 μs pulse repetition interval), in a temperature range from 15 °C to 50 °C are given in Fig. 4.

To measure the optical spectrum of the device, we coupled the hybrid laser output into a single-mode fiber connected to an optical spectrum analyzer. Typical optical spectrum of the
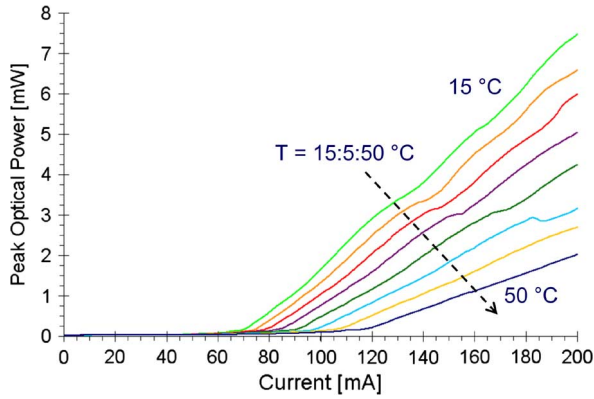
Fig. 4.   *L–I* plots of the hybrid laser (900 μm-long cavity) in pulsed regime (5% duty cycle, 100-μs pulse repetition interval).

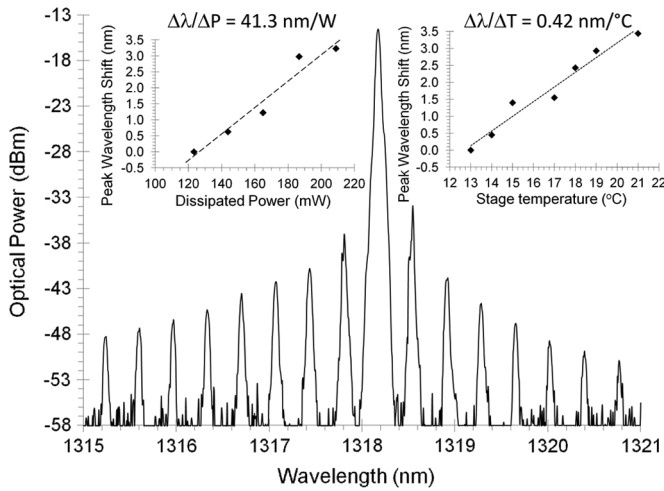
Fig. 5.   Optical spectra of the hybrid laser (CW regime, 120 mA injected current, 700 μm-long device). Inserted are the plots of peak wavelength shifts versus dissipated power (top left) and stage temperature (top right).

laser in CW regime is given in Fig. 5. Longitudinal modes of a Fabry–Pérot laser are clearly visible with the peak wavelength at 1318.18 nm. The mode spacing is 0.37 nm, corresponding to a group index of 3.35 (for a 700 μm-long device). Optical power measurements in CW regime (Fig. 3) suggest relatively high thermal impedance (R_{th}) of the device, due to a strong rollover and lack of lasing at temperatures of 25 °C and above. To assess R_{th}, using the method described in [10], we have performed a series of optical spectral measurements in both CW and pulsed regimes and observed the shift in peak lasing wavelength ($\Delta\lambda$). In CW regime, we measured $\Delta\lambda$ versus dissipated power in the device, while in the pulse regime (1% duty cycle, 100 μs pulse repetition interval) we measured $\Delta\lambda$ versus the temperature of the stage (controlled using a Peltier element). Results of these measurements are inserted in Fig. 5. Using a linear fit, we measure a wavelength shift with the increase of dissipated power of $\Delta\lambda/\Delta P = 41.3$ nm/W, while the wavelength shift with the increase of the temperature of the stage is

$\Delta\lambda/\Delta T = 0.42$ nm/°C. This yields a value for the thermal impedance of 95.3 K/W, which is higher than 41.8 K/W that was reported for the direct wafer bonding hybrid III–V/Si laser [10]. The main reason for such a high R_{th} value is the presence of 50 nm-thick DVS-BCB bonding layer with the low thermal conductivity (0.3 W/m · K), compared to 5 nm-thick SiO$_2$ layer (1.3 W/m · K thermal conductivity) that is present at the III–V/Silicon interface of the direct wafer bonding hybrid III–V/Si laser [2].

V. CONCLUSION

We have demonstrated, for the first time, evanescent hybrid III–V/silicon Fabry–Pérot lasers, based on DVS-BCB adhesive bonding, emitting at 1310 nm. The devices were fabricated using a specially developed die-to-die DVS-BCB bonding technique, offering more relaxed bonding conditions compared to direct bonding. Lasing in both CW and pulse regime was demonstrated, with a relatively high thermal impedance being observed and assessed using optical spectra measurements. Ways to improve thermal properties of the lasers will be pursued, primarily by adding a thermal via or flip-chipping the fabricated devices upside down on a silicon substrate that serves as a heat sink. The thin BCB bonding process will be scaled up to bond multiple III–V dies to wafer which will allow large-scale integration of hybrid lasers on wafers with photonic integrated circuits.

REFERENCES

[1] M. Lamponi *et al.*, "Heterogeneously integrated InP/SOI laser using double tapered single-mode waveguides through InP die to SOI wafer bonding," in *Proc. 7th IEEE Int. Conf. Group IV Photonics*, Beijing, 2010, p. Paper WB6.

[2] A. W. Fang, H. Park, R. Jones, O. Cohen, M. J. Paniccia, and J. E. Bowers, "A continuous-wave hybrid AlGaInAs–silicon evanescent laser," *IEEE Photon. Technol. Lett.*, vol. 18, no. 10, pp. 1143–1145, May 15, 2006.

[3] H.-H. Chang *et al.*, "1310 nm silicon evanescent laser," *Opt. Express*, vol. 15, no. 18, pp. 11466–11470, Aug. 2007.

[4] X. Sun *et al.*, "Electrically pumped hybrid evanescent Si/InGaAsP lasers," *Opt. Lett.*, vol. 34, no. 9, pp. 1345–1347, May 2009.

[5] A. W. Fang *et al.*, "A distributed Bragg reflector silicon evanescent laser," *IEEE Photon. Technol. Lett.*, vol. 20, no. 20, pp. 1667–1669, Oct. 15, 2008.

[6] A. W. Fang, E. Lively, Y. Kuo, D. Liang, and J. E. Bowers, "A distributed feedback silicon evanescent laser," *Opt. Express*, vol. 16, no. 7, pp. 4413–4419, Mar. 2008.

[7] T. Hong *et al.*, "A selective-area metal bonding InGaAsP–Si laser," *IEEE Photon. Technol. Lett.*, vol. 22, no. 15, pp. 1141–1143, Aug. 1, 2010.

[8] G. Roelkens, D. Van Thourhout, R. Baets, R. Nötzel, and M. Smit, "Laser emission and photodetection in an InP/InGaAsP layer integrated on and coupled to a silicon-on-insulator waveguide circuit," *Opt. Express*, vol. 14, no. 18, pp. 8154–8159, Sep. 2006.

[9] S. Stanković, R. Jones, J. Heck, M. Sysak, D. Van Thourhout, and G. Roelkens, "Die-to-die adhesive bonding for evanescently-coupled photonic devices," *Electrochem. Solid-State Lett.*, vol. 14, no. 8, pp. H326–H329, May 2011.

[10] M. N. Sysak *et al.*, "Experimental and theoretical thermal analysis of a hybrid silicon evanescent laser," *Opt. Express*, vol. 15, no. 23, pp. 15041–15046, Nov. 2007.